Cellular Effects of Small Molecule PTP1B Inhibitors on Insulin Signaling †

ARTICLE *in* BIOCHEMISTRY · DECEMBER 2003

Impact Factor: 3.02 · DOI: 10.1021/bi035238p · Source: PubMed

Cellular Effects of Small Molecule PTP1B Inhibitors on Insulin Signaling†

Laiping Xie,[‡,§] Seung-Yub Lee,[‡,§] Jannik N. Andersen,[||,⊥] Steve Waters,[@] Kui Shen,[#,+] Xiao-Ling Guo,[‡] Niels Peter H. Moller,[||] Jerrold M. Olefsky,[○] David S. Lawrence,*[,#] and Zhong-Yin Zhang*[,‡,#]

Department of Molecular Pharmacology and Department of Biochemistry, Albert Einstein College of Medicine, 1300 Morris Park Avenue, Bronx, New York 10461, Department of Signal Transduction, Novo Nordisk, DK-2880 Bagsaerd, Denmark, Metabolex, Inc., 3878 Bay Center Plaza, Hayward, California 94545, and Department of Medicine, University of California at San Diego, La Jolla, California 92093

Received July 14, 2003; Revised Manuscript Received September 4, 2003

ABSTRACT: Protein tyrosine phosphatase 1B (PTP1B) is implicated as a negative regulator of insulin receptor (IR) signaling and a potential drug target for the treatment of type 2 diabetes and other associated metabolic syndromes. To further define the role of PTP1B in insulin signaling and to test the hypothesis that blocking the activity of PTP1B would augment the action of insulin, we prepared several cell permeable, potent and selective, small molecule PTP1B inhibitors, and evaluated their biological effects in several insulin sensitive cell lines. Our data indicate that PTP1B inhibitors bind to and colocalize with PTP1B on the surface of the endoplasmic reticulum and PTP1B exerts its negative effect on insulin signaling upstream of phosphatidylinositol 3-kinase and MEK1. Treatment of cells with PTP1B inhibitors, both in the presence and in the absence of insulin, markedly enhances IRβ and IRS-1 phosphorylation, Akt and ERK1/2 activation, Glut4 translocation, glucose uptake, and Elk1 transcriptional activation and cell proliferation. These results indicate that small molecule inhibitors targeted to PTP1B can act as both insulin mimetics and insulin sensitizers. Taken together, our findings combined with results from PTP1B knockout, antisense, and biochemical studies provide strong evidence that PTP1B negatively regulates insulin signaling and that small molecule PTP1B inhibitors have the ability to potentiate and augment the action of insulin.

Tyrosine phosphorylation is a key reaction in the initiation and propagation of insulin action (*1*, *2*). Insulin exerts its pleiotropic effects by binding to its receptor on insulin target tissues (adipose, liver, and muscle). Insulin binding to the insulin receptor (IR)[1] induces activation of the intrinsic tyrosine kinase activity in the β-subunit (IRβ), which is followed by autophosphorylation of at least six tyrosine residues within three distinct regions of IRβ. The activated IR then recruits and phosphorylates insulin receptor substrates (IRS-1−4) and other adapter proteins (Gab1 and Shc) that mediate the biological effects of insulin (*3*, *4*). The phosphorylation on tyrosine residues in IR and IRS proteins generates docking sites for other enzymes and effector molecules containing SH2 or phosphotyrosine-binding domains to propagate the insulin signal.

A key enzyme essential for the cellular and metabolic responses triggered by insulin stimulation is phosphatidylinositol 3-kinase (PI3K) (*5*, *6*). Engagement of the SH2 domain in the regulatory subunit of PI3K to the IRS proteins results in the activation of the PI3K catalytic subunit, which initiates a cascade of reactions leading to the phosphorylation and activation of the Ser/Thr protein kinase Akt/PKB. Activated Akt stimulates glucose uptake in muscle and adipocytes, which is mediated by translocation of the insulin sensitive glucose transporter Glut4 vesicles to the plasma membrane (*7*−*9*). To promote the mitogenic effect of insulin, the adapter protein Shc, upon phosphorylation by IR, forms

† This work was supported by NIH Grant GM55242 and the G. Harold and Leila Y. Mathers Charitable Foundation. L.X. was supported in part by a fellowship from AstraZeneca. J.N.A. was supported by an industrial Ph.D. fellowship from the Danish Academy of Technical Sciences and Novo Nordisk. Z.-Y.Z. is an Irma T. Hirschl Career Scientist.

* To whom correspondence should be addressed. E-mail: dlawrenc@aecom.yu.edu (D.S.L.) and zyzhang@aecom.yu.edu (Z.-Y.Z.).

‡ Department of Molecular Pharmacology, Albert Einstein College of Medicine.

§ These authors contributed equally to this work.

|| Novo Nordisk.

⊥ Present address: Cold Spring Harbor Laboratory, 1 Bungtown Rd., Cold Spring Harbor, NY 11724.

@ Metabolex, Inc.

Department of Biochemistry, Albert Einstein College of Medicine.

+ Present address: Department of Pharmacology, Johns Hopkins University School of Medicine, 725 N. Wolfe St., Baltimore, MD 21205.

○ University of California at San Diego.

[1] Abbreviations: CHO/HIRc, Chinese hamster ovary cell line transfected with an expression plasmid encoding the human insulin receptor; DMF, dimethylformamide; DIPEA, diisopropylethylamine; DMA, dimethylacetamide; DMSO, dimethyl sulfoxide; ER, endoplasmic reticulum; ERK, extracellular signal-regulated protein kinase; ESI-MS, electrospray ionization mass spectroscopy; FCS, fetal calf serum; Fmoc, 9-fluorenylmethoxycarbonyl; FMPB AM resin, 4-(4-formyl-3-methoxyphenoxy)butyryl AM resin; Grb2, growth factor receptor-bound protein 2; HPLC, high-performance liquid chromatography; HRP, horseradish peroxidase; IR, insulin receptor; IRβ, insulin receptor β-subunit; IRS, insulin receptor substrate; Lissamine, rhodamine B sulfonyl chloride; MAP kinase, mitogen-activated protein kinase; MEK, MAP kinase/ERK kinase; MALDI-TOF, matrix-assisted laser desorption ionization time-of-flight; MS, mass spectroscopy; NMR, nuclear magnetic resonance; PI3K, phosphatidylinositol 3-kinase; PTP, protein tyrosine phosphatase; pTyr, phosphotyrosine; PTP1B, protein tyrosine phosphatase 1B; Shc, Src-homology 2-containing transforming protein; SOS, son-of-sevenless; TFA, trifluoroacetic acid; TIS, triisopropylsilane.

10.1021/bi035238p CCC: $25.00
Published on Web 10/17/2003

a complex with Grb2 and the guanine nucleotide exchange factor SOS, which is required for ras activation in response to insulin. Activation of the ras/MAP kinase pathway is essential for the mitogenic effects of insulin, but is not required for insulin-stimulated glucose transport (*10*).

The termination of insulin action, upon insulin withdrawal, consequently requires the dephosphorylation of both the insulin receptor and insulin receptor substrates by protein tyrosine phosphatases (PTPs). Several PTPs have been suggested as negative regulators of insulin-initiated pathways (*11*). Among these, PTP1B has emerged as a key player that negatively regulates insulin signaling. PTP1B is capable of interacting with and removing tyrosine phosphates from both IR and IRS proteins (*12*−*17*). Overexpression of PTP1B in cell cultures decreases the level of insulin-stimulated IRβ and/or IRS-1 phosphorylation, while reduction of the level of PTP1B by antisense oligonucleotides or neutralizing antibodies augments the insulin-initiated signaling pathways (*18*−*20*). Moreover, PTP1B-deficient mice display increased or prolonged phosphorylation in IRβ and IRS-1 in skeletal muscle and liver, and the mutant mice exhibit increased insulin sensitivity and resistance to diet-induced obesity (*21*, *22*). Collectively, the data implicate PTP1B as an attractive target for the treatment of type 2 diabetes and obesity.

There are currently few examples of a direct association of PTPs with diseases, and clearly, the credibility of these enzymes as targets for drug design requires substantial and continued validation. As a prerequisite for the clinical development of therapeutics targeted to PTP1B, it is important to determine the cellular effects of small molecule PTP1B inhibitors. Unfortunately, as a consequence of the conserved nature of the PTP active sites (i.e., pTyr binding sites), there are currently few PTP1B inhibitors that exhibit the potency and specificity required for biological and pharmacological investigation. On the basis of the observation that PTP substrate recognition requires both pTyr and its adjacent flanking residues (*23*) and the discovery of a second aryl phosphate-binding site adjacent to the active site in PTP1B (*24*), we have focused on a strategy for developing bidentate PTP inhibitors that bind to both the active site and a unique adjacent peripheral site. Using this approach, we have obtained several small molecule PTP1B inhibitors, some of which represent the most potent and selective PTP1B inhibitors reported to date (*25*−*28*). In the study presented here, we have evaluated the cellular effects of these small molecule PTP1B inhibitors on insulin signaling in several insulin sensitive cell lines. Our results show that small molecule PTP1B inhibitors can serve as both insulin mimetics and sensitizers, validating the notion that small molecule PTP1B inhibitors could be used as anti-diabetes therapeutics. Since PTP1B is also involved in the regulation of other signaling pathways, these potent and specific PTP1B inhibitors should be useful reagents in helping to define the role of PTP1B in normal physiology and disease states.

EXPERIMENTAL PROCEDURES

General Procedures. All moisture sensitive reactions were carried out in oven-dried glassware under a positive pressure of dry N_2 or Ar. DMA, DMF, CH_2Cl_2, and tetrahydrofuran for moisture sensitive reactions were purchased from Aldrich in Sure/Seal bottles. All reactions were followed by thin layer chromatography using E. Merck silica gel 60 °F-254. Flash column chromatography was performed using J. T. Baker silica gel (230−400 mesh). Benzotriazol-1-yloxy-tris(dimethylamino)phosphonium hexafluorophosphate, 1,3-diisopropylcarbodiimide, 1-hydroxybenzotriazole, piperidine, benzotriazol-1-yloxy-tris(pyrrolidino)phosphonium hexafluorophosphate, tetramethylfluoroformamidinium hexafluorophosphate, and *O*-(*N*-succinimidyl)-1,1,3,3-tetramethyluronium tetrafluoroborate for peptide synthesis were purchased from Advanced ChemTech. *O*-(7-Azabenzotriazol-1-yl)-*N*,*N*,*N*′,*N*′-tetramethyluronium hexaflurophosphate was purchased from Aldrich. ϵ-Maleimidocapric acid was purchased from Sigma. Lissamine (rhodamine B sulfonyl chloride) was purchased from Molecular Probes. FMPB AM resin was purchased from NOVA Biochem. The structures of new compounds were characterized by ^{1}H NMR (300 MHz), ^{13}C NMR (75.5 MHz), ^{19}F NMR (282 MHz), and ^{31}P NMR (121 MHz) at 299 K unless otherwise indicated, and by ESI-MS analysis.

*Preparation of Precursors to Compounds **II** and **III**.* *N*-Fmoc-4-(difluorophosphonomethyl)-L-phenylalanine (**1**) was prepared via literature procedures (*26*, *29*), and 4-(phosphonodifluoromethyl)phenylacetic acid (**5**) was prepared as described below.

Synthesis of Benzyl 4-[(Diethoxyphosphoryl)difluoromethyl]phenyl Acetate. A solution of diethyl bromodifluorophosphonate (8.54 g, 32.0 mmol) in DMA (10 mL) was added slowly to zinc powder (522 mg, 8.0 mmol) in DMA (10 mL), and the reaction mixture was stirred for 1 h. Cuprous bromide (1.15 g, 8.0 mmol) was added in one portion, and the mixture was stirred for 1 h. A solution of (4-iodophenyl)acetic acid benzyl ester (2.82 g, 8.0 mmol) in DMA (10 mL) was added dropwise, and the resulting mixture was sonicated for 24 h at room temperature. The reaction mixture was diluted with EtOAc, washed with brine, dried over $MgSO_4$, filtered, and concentrated with rotary evaporation. The crude oil was chromatographed on silica gel using hexanes and EtOAc (5:1) as an eluant to give benzyl 4-[(diethoxyphosphoryl)difluoromethyl]phenyl acetate (2.14 g, 65% yield) as a viscous colorless oil: ^{1}H NMR (300 MHz, $CDCl_3$) δ 1.27 (t, 6H, J = 7.2 Hz, $OCH_2C\underline{H}_3$), 3.68 (s, 2H, $ArC\underline{H}_2CO$), 4.14 (m, 6H, $OC\underline{H}_2CH_3$), 5.11 (s, 2H, $COOC\underline{H}_2Ph$), 7.32 (m, 5H, $\underline{H}$-Ar), 7.35 (d, 2H, J = 8.2 Hz, $\underline{H}$-Ar), 7.57 (d, 2H, J = 8.2 Hz, $\underline{H}$-Ar); ^{13}C NMR (75 MHz, $\underline{C}DCl_3$) δ 15.96, 16.03, 40.71, 64.40, 64.49, 66.42, 118.05 (m), 126.20 (m), 127.82, 127.98, 128.26, 129.15, 131.25 (m), 135.44, 136.60, 170.32; ^{31}P NMR (121.5 MHz, $CDCl_3$) δ 7.49 (t, J = 116.6 Hz); ^{19}F NMR (282 MHz, $CDCl_3$) δ −108.60 (d, J = 116.6 Hz).

Synthesis of {4-[(Diethoxyphosphoryl)difluoromethyl]-phenyl}acetic Acid. A solution of LiOH (235 mg, 5.6 mmol) in H_2O (28 mL) was added to a solution of benzyl 4-[(diethoxyphosphoryl)difluoromethyl]phenyl acetate (1.17 g, 2.8 mmol) in tetrahydrofuran (20 mL), and the reaction mixture was stirred at 0 °C for 3 h. A saturated $NaHCO_3$ solution (10 mL) was added, and the crude mixture was extracted with EtOAc (2 × 25 mL). A 2 N HCl solution was added to neutralize the base, and the resulting mixture was extracted with EtOAc (2 × 50 mL). The combined EtOAc extracts were washed with brine, dried over Na_2SO_4, filtered, and concentrated. The crude colorless oil was used for the next step: ^{1}H NMR (300 MHz, $CDCl_3$) δ 1.30 (t, 6H, J = 7.2 Hz, $OCH_2C\underline{H}_3$), 3.67 (s, 2H, $ArC\underline{H}_2CO$), 4.14

(m, 6H, $OC\underline{H}_2CH_3$), 7.37 (d, 2H, J = 8.2 Hz, $\underline{H}$-Ar), 7.57 (d, 2H, J = 8.2 Hz, $\underline{H}$-Ar); ^{13}C NMR (75 MHz, $CDCl_3$) δ 16.20, 16.28, 40.71, 64.95, 65.04, 118.05 (m), 126.20 (m), 129.48, 131.25 (m), 136.50, 175.55; ^{31}P NMR (121.5 MHz, $CDCl_3$) δ 7.39 (t, J = 116.6 Hz); ^{19}F NMR (282 MHz, $CDCl_3$) δ −108.80 (d, J = 116.6 Hz).

*Synthesis of 4-(Phosphonodifluoromethyl)phenylacetic Acid (**5**).* Trimethylsilyl bromide (1.224 g, 8.0 mmol) was added to a solution of {4-[(diethoxyphosphoryl)difluoromethyl]-phenyl}acetic acid (644 mg, 2.0 mmol) in anhydrous CH_2Cl_2 (5 mL), and the reaction mixture was stirred for 20 h at room temperature. NH_4HCO_3 in H_2O (158 mg, 8.0 mmol in 2 mL) was added slowly to the reaction mixture, and the crude solution was concentrated by rotary evaporation. The resultant oil was lyophilized to give **5** as a white solid (530 mg, 99% yield): ^{1}H NMR (300 MHz, D_2O) δ 3.49 (s, 2H, $ArC\underline{H}_2COOH$), 7.25 (d, 2H, J = 8.6 Hz, $\underline{H}$-Ar), 7.48 (d, 2H, J = 8.6 Hz, $\underline{H}$-Ar); ^{13}C NMR (75 MHz, D_2O) δ 40.752, 121.72 (m), 126.54 (m), 129.84, 133.25 (m), 133.63, 176.90; ^{31}P NMR (121.5 MHz, D_2O) δ 6.37 (t, J = 97.6 Hz); ^{19}F NMR (282 MHz, D_2O) δ −106.30 (d, J = 97.6 Hz); ESI-MS calcd mass (M) 266.1, found (M^+) 266.6.

*Synthesis of **14**.* FMPB AM resin (Nova Biochem) (500 mg, 0.49 mmol) **7** was swollen in dichloroethane (5 mL) and trimethyl orthoformate (3 mL) for 1 h. Tetradecylamine (1.569 g, 7.35 mmol) and $NaBH(OAc)_3$ (1.56 g, 7.35 mmol) were added, and the reaction mixture was stirred at room temperature for 12 h under an N_2 atmosphere. The resin was sequentially washed with DMF, 10% DIPEA and 90% DMF, and DMF. The amine resin was reacted with the mixture of *N*-α-Fmoc-*N*-ϵ-4-methyltrityl-L-lysine (3.123 g, 5.0 mmol) **9**, *O*-(7-azabenzotriazol-1-yl)-*N*,*N*,*N*′,*N*′-tetramethyluronium hexaflurophosphate (1.9 g, 5 mmol), and DIPEA (1.293 g, 10.0 mmol) for 3 h. After the coupling reaction was complete, the methyltrityl group was removed with the mixture of CH_2Cl_2 (20 mL), TFA (0.3 mL), and TIS (1 mL), and then the resin was subsequently treated with a mixture of 10 equiv of Lissamine **11** and DIPEA in DMF for 10 h. After completion of the Lissamine coupling, the resin (200 mg, 0.1 mmol) was exposed to 30 mL of 20% piperidine (30 min) in DMF to remove the Fmoc group. The peptide resin was subsequently treated with a mixture of ϵ-maleimidocaproic acid (210 mg, 1.0 mmol) **12**, *O*-benzotriazol-1-yl-*N*,*N*,*N*′,*N*′-tetramethyluronium hexafluorophosphate (379 mg, 1.0 mmol), and *N*-methylmorpholine (202 mg, 2.0 mmol). The peptide was deprotected and cleaved via treatment with a 95% TFA/2.5% water/2.5% TIS mixture at room temperature for 3 h. Removal of the solvent *in vacuo* gave a crude oil that was triturated with cold ether. The crude mixture thus obtained was centrifuged, the ether removed by decantation, and the resulting white solid purified by semipreparative reverse phase HPLC (H_2O/CH_3CN/0.1% TFA). Peptide **14** was obtained as a reddish solid by lyophilization and characterized by mass spectrometry: ESI-MS calcd mass (M) 1075.4, found ($[M + H]^+$) 1076.5.

*Synthesis of Compound **II**.* Synthesis of compound **II** was performed on Rink amide resin using a standard *O*-benzotriazol-1-yl-*N*,*N*,*N*′,*N*′-tetramethyluronium hexafluorophosphate/1-hydroxybenzotriazole/*N*-methylmorpholine protocol for the activation of carboxylic acids. The coupling reaction was performed in DMF for 2 h using a 3-fold excess of acid relative to resin-bound amine. *N*-Fmoc-4-(difluorophosphonomethyl)-L-phenylalanine (**1**), *N*-Fmoc-L-aspartic acid β-*tert*-butyl ester (**2**), compound **1**, and *n*-pentadecanoic acid were sequentially coupled to the Rink amide resin. Fmoc removal after each coupling was effected with 20% piperidine in DMF. Final cleavage and side chain deprotection were achieved by treatment with a 94% TFA/5% 1,2-ethanedithiol/1% *m*-cresol mixture at room temperature for 3 h. Removal of the solvent *in vacuo* gave a crude oil that was triturated with cold ether. The crude mixture thus obtained was centrifuged, the ether removed by decantation, and the resulting white solid purified by semipreparative reverse phase HPLC (H_2O/CH_3CN/0.1% TFA). Compound **II** was obtained as a white solid by lyophilization: ^{1}H NMR (300 MHz, DMSO) δ 1.25 [t, 3H, J = 6.4 Hz, $C\underline{H}_3(CH_2)_{12}CH_2$-CO], 1.63 [m, 24H, $CH_3(C\underline{H}_2)_{12}CH_2CO$], 2.42 [t, 2H, J = 7.1 Hz, $CH_3(CH_2)_{12}C\underline{H}_2CO$], 3.06−3.50 (m, 6H, $C\underline{H}_2COOH$ and $C\underline{H}_2Ar$), 4.78−4.92 (m, 3H, $NHC\underline{H}RCO$), 7.71 (d, 2H, J = 8.0 Hz, $\underline{H}$-Ar), 7.74 (d, 2H, J = 8.0 Hz, $\underline{H}$-Ar), 7.81 (d, 4H, J = 8.0 Hz, $\underline{H}$-Ar); ^{13}C NMR (75 MHz, DMSO) δ 14.13, 22.17, 25.14, 28.62, 28.79 (2C), 28.84, 28.95, 29.11 (2C), 29.15 (2C), 31.37, 35.23 (2C), 35.89, 36.88, 37.26, 49.92, 53.83, 125.95 (2C), 128.94 (8C), 132.20 (m, 2C), 140.15 (2C), 170.32, 171.77, 172.05, 172.47, 172.67; ^{31}P NMR (121.5 MHz, DMSO) δ 4.2 (t, J = 107.7 Hz), 4.4 (t, J = 108.0 Hz); ^{19}F NMR (282 MHz, DMSO) δ −107.93 (d, J = 107.7 Hz), −107.80 (d, J = 108.0 Hz); HRMS calcd mass ($M + H^-$ peak) for $C_{39}H_{57}F_4N_4O_{12}P_2$ 909.3228, found 909.3191 (Δ = 4.1 ppm).

*Synthesis of Compound **III**.* Compound **6** (9 mg) (*28*) in a triethylammonium acetate buffer solution (pH 8.0, 2 mL) was added to the mixture of **14** (10 mg) and CH_3CN (2 mL) at room temperature, and the reaction mixture was stirred at room temperature for 12 h. Compound **III** was purified by semipreparative reverse phase HPLC (H_2O/CH_3CN/0.1% TFA) and subsequently obtained as a reddish solid by lyophilization. Compound **III** was characterized by mass spectrometry: ESI-MS calcd mass (M) 1949.1, found (M^+) 1949.8.

Antibodies and Chemicals. Monoclonal anti-pTyr antibody 4G10 and PI-3 kinase inhibitor wortmannin were from Upstate Biotechnology, Inc. (Lake Placid, NY). Monoclonal anti-pTyr antibody PY20 conjugated with HRP, anti-IRβ (insulin receptor β) and anti-IRS-1 (insulin receptor substrate 1) conjugated with HRP, polyclonal anti-IRβ and polyclonal anti- IRS-1 conjugated with agarose beads, and goat serum were all from Santa Cruz Biotechnology (Santa Cruz, CA). Rabbit polyclonal anti-ERK1/2, polyclonal anti-phospho-ERK1/2, polyclonal anti-phospho-Akt1, secondary anti-mouse as well as anti-rabbit IgG (H+L) linked with HRP, and the ECL developing system were bought from Cell Signaling Technology. Rabbit anti-GRP78 polyclonal antibody was from Research Diagnostics, Inc. (Flanders, NJ), and the anti-rabbit IgG F(ab′) fragment labeled with Cy5 was from Jackson ImmunoResearch Laboratories, Inc. (West Grove, PA). Bovine insulin, MEK inhibitor U0126, sodium orthovanadate, Tween 20, and Triton X-100 were purchased from Sigma. Compound **I** was synthesized as described previously (*26*).

Cell Lines and Tissue Culture. The Chinese hamster ovary (CHO) cell line transfected with an expression plasmid encoding the human insulin receptor (CHO/HIRc) was a generous gift from J. Backer (Albert Einstein College of

Medicine). The cells were maintained in Ham's F-12 medium containing 10% fetal calf serum (FCS) and were cultured to confluence in 100 mm, 60 mm, or six-well plates. The rat L6 myoblast cell line was obtained from ATCC (CRL-1458). L6 myoblast cells were grown and maintained in minimum Eagle's medium-a containing 50 units of penicillin/mL, 50 μg/mL streptomycin, and 10% FBS in a 5% CO_2 environment. For the differentiation of L6 myoblasts, cells were reseeded in appropriate culture dishes, and after the cells had reached subconfluency, the medium was changed to minimum Eagle's medium containing 2% FCS. The medium was then changed every 2 days until the cells were fully differentiated, normally in 8−11 days (*30*).

Tyrosine Phosphorylation of IRβ and IRS-1 in CHO/HIRc Cells. Nearly confluent CHO/HIRc cells were serum starved overnight with Ham's F-12 medium without serum. The cells were then treated for 1 h with a range of compound **II** concentrations, followed by stimulation with or without 10 nM insulin for 5 min. The incubation was terminated by removing the fluid and immersing the dishes in liquid nitrogen. Cells were scraped and lysed with lysis buffer [50 mM Tris-HCl (pH 7.5), 5 mM EDTA, 150 mM NaCl, 1% Triton X-100, 5 mM iodoacetic acid, 10 mM sodium phosphate, 10 mM NaF, 5 mg/mL leupeptin, 5 mg/mL aprotinin, and 1 mM benzamidine]. The clarified cell lysates were incubated with anti-IRβ or anti-IRS-1 polyclonal antibodies conjugated with agarose beads [1:15 dilution of a 50% slurry in 1% Nonidet P-40, 0.5% Triton X-100, 10% glycerol, and 150 mM Tris-HCl (pH 7.4)]. After overnight incubation at 4 °C, the immunocomplexes were resolved by SDS−PAGE, eletrotransferred to nitrocellulose membranes, and probed with anti-pTyr antibody. The membrane was stripped and reprobed with anti-IRβ or anti-IRS-1 antibodies. The blots were developed using the ECL chemiluminescence detection system.

Phosphorylation of ERK1/2 and Akt1 in CHO/HIRc Cells and in L6 Myotubes. Cells were starved overnight with Ham's F-12 medium (for CHO/HIRc cells) or minimum Eagle's medium-a (for L6 myotubes) without serum, and the cells were treated with compound **II** and insulin as described above. The clarified cell lysates were subjected to SDS−PAGE under reducing conditions. After electrotransfer, nitrocellulose membranes were incubated with anti-phospho-Akt1 antibodies (1:2000) or anti-phospho-ERK1/2 antibodies (1:2000) in nonfat dry milk at 4 °C overnight. The membranes were reprobed with anti-rabbit IgG conjugated with HRP. The films were developed with an ECL system.

Elk1 Activation in CHO/HIRc Cells. Quantification of Elk1 activation was determined using PathDetect Elk1 Trans-Reporting System according to the manufacturer's protocol. The assay is designed to detect endogenous ERK activity *in vivo*. The pFA-Elk1 vector expresses a fusion protein of the functional domain of Elk1 and the GAL4 DNA binding domain. The reporter vector, pFR-Luc, contains a GAL4-response element upstream of the luciferase gene. Phosphorylation of Elk1 by ERK causes Elk1 homodimerization that induces DNA binding through the GAL4 responsive element, and results in the activation of the reporter gene. For this experiment, CHO/HIRc cells in six-well plates were transiently cotransfected with 100 ng of pFA-Elk1 and 0.5 μg of pFR-Luc by the LIPOTAXI method. pCMV-Beta gal (from Stratagene) with 100 ng was also cotransfected to monitor the transfection efficiency. Eighteen to twenty hours after transfection, the cells were serum starved for 4 h and then incubated with or without 10 nM bovine insulin together with varying concentrations of compound **II** for 30 h. Cell lysates were prepared and assayed for luciferase activity using the luciferase assay system (Promega Corp., Madison, WI). Light emission was measured for 12−24 s with a luminometer.

Cell Proliferation Assay. CHO/HIRc cells were seeded into 96-well plate at a concentration of 2×10^3 cells/well and incubated at 37 °C in 5% CO_2 for 24 h, and then the medium was changed to 100 μL of F-12 Ham's medium containing 2% FCS. A range of concentrations of inhibitor were added to 96-well plates with or without 10 nM bovine insulin, and the plates were incubated at 37 °C for 48 h. The cell proliferation rate was measured by a CellTiter 96 Aqueous One Solution Cell Proliferation Assay kit (Promega). OD values were read at 490 nm.

Measurement of the Rate of 2-Deoxy-D-glucose Uptake in CHO/HIRc Cells. 2-Deoxyglucose uptake by CHO/HIRc cells was assessed according to a published method (*31*). CHO/HIRc cells were seeded into a 24-well plate at a concentration of 1.5×10^5 cells/well with F-12 Ham's medium containing 10% FCS. Nearly confluent monolayers of the cells were incubated in serum free Ham's F-12 medium for 3−4 h. Then, cells were washed rapidly three times with Krebs-Ringer Phosphate (KRP) buffer (pH 7.4), and 450 μL of KRP buffer was added to each well. The cells were first treated with compound **II** (500 nM) for 1 h. Subsequently, the cells were stimulated without or with a series of insulin concentrations for 30 min. The measurements of the rate of 2-deoxyglucose uptake were initiated by the addition of 50 μL of 2-deoxy[1,2-^{3}H]glucose (NEN, Inc.) stock so that each well contained 0.4 μCi and 0.1 mM glucose. After incubation for 1 min at 37 °C, 1 mL of 10 mM ice-cold phosphate-buffered saline (PBS) containing 10 mM glucose and 0.3 mM phloretin (Sigma) (*32*) was added. Cells were rapidly washed three times with ice-cold PBS containing 10 mM glucose, and solubilized by the addition of SDS (at a final concentration of 0.05%). Aliquots of the solubilized extract were measured for radioactivity.

Measurement of the Rate of 2-Deoxyglucose Uptake in L6 Myotubes. L6 myotubes were deprived of serum and incubated in minimal essential medium containing 5.5 mM glucose for 5 h at 37 °C. For the effect of compound **II** on basal glucose uptake, the cells were treated with 50 nM, 125 nM, and 1.25 μM compound **II** for 1 h in the absence of insulin. To determine the effect of compound **II** on the insulin dose−response curve, L6 myotubes were treated with 125 nM **II** (1 h) and stimulated with a range of insulin concentrations for 30 min. Cells were rinsed twice rapidly with a glucose-free Hepes-buffered saline solution [140 mM NaCl, 25 mM $MgSO_4$, 1 mM $CaCl_2$, 5 mM KCl, 1 mg/mL BSA, and 20 mM Hepes-Na (pH 7.4)], followed by addition of 2-deoxy[1,2-^{3}H]glucose (final concentration of 1 μCi and 0.1 mM glucose) for 3 min in the same solution at 37 °C with incessant shaking. Transport was terminated by aspiration of the radioactive solution followed by three rapid wash steps with cold PBS containing 10 mM glucose. Radioactivity inside the cells was measured after cell rapture with 0.05 M NaOH. The level of non-carrier-mediated glucose uptake was determined in parallel samples in the presence of 5 μM

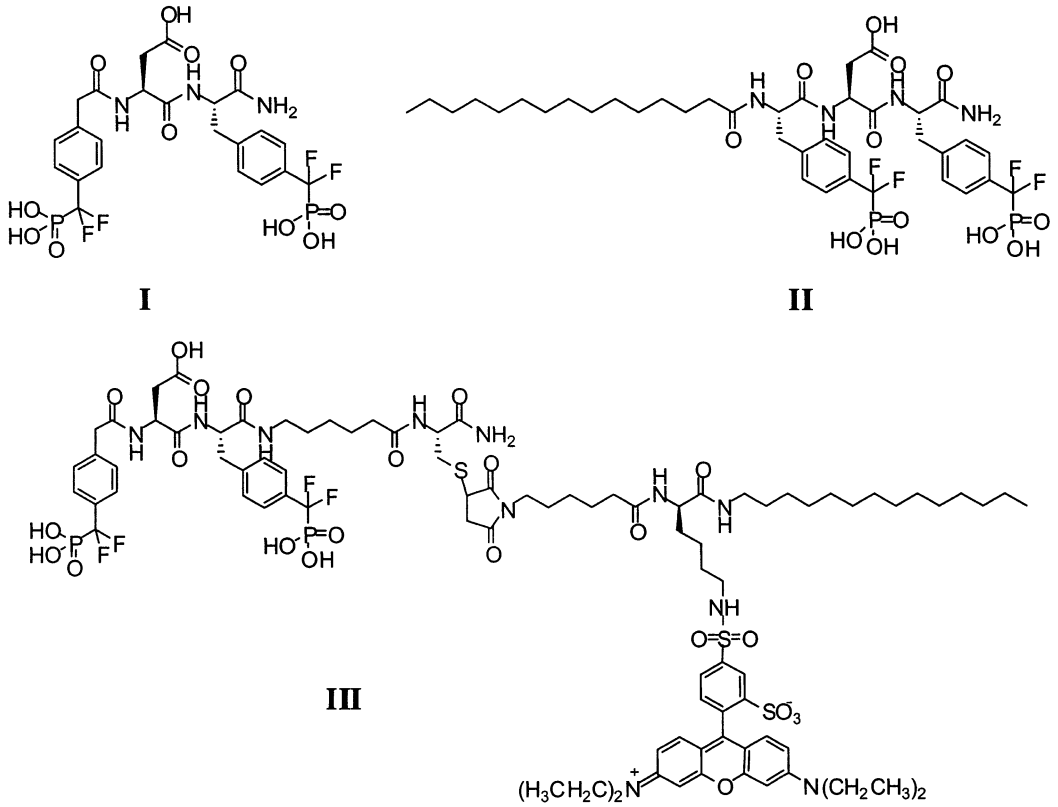

FIGURE 1: Chemical structures of compounds **I**−**III**.

cytochalasin B (*33*), and was subtracted from all measurements. The protein concentration was determined with the BCA protein assay kit (Pierce). The radioactivity measurements were normalized with the protein levels.

Fluorescence Microscopy. To determine the cell permeability of rhodamine-labeled compound **III**, cells were treated with **III** (1 μM) for 1 h. Subsequently, the cells were washed once with cold PBS, fixed with a fresh formaldehyde solution for 10 min at room temperature, and rinsed three times with cold PBS. The cells were observed and photos taken with a fluorescent confocal microscope. For colocalization experiments, full-length human PTP1B inserted into the multiple cloning sites of the C-terminally enhanced green fluorescent protein expression vector pEGFP-C3 (a generous gift from C.-W. Chow, Albert Einstein College of Medicine) was used. CHO/HIRc cells were seeded onto cover slips inside the six-well plates, and cultured at 37 °C with 5% CO_2 overnight. CHO/HIRc cells were transfected via the LipoTAXI transfection reagent (Stratagene, Cedar Creek, TX) with 4 μg of plasmid DNA for each well. After 3 h, the cells were returned to normal growth medium for 30 h. Thereafter, the cells were incubated with **III** at a final concentration of 1 μM for 1 h. The cells were washed three times and fixed with 3.7% paraformaldehyde in PBS (pH 7.4) for 15 min. The cells were permeabilized with 0.1% Triton X-100 in PBS for 10 min, followed by a 30 min incubation at room temperature with blocking solution (0.2% BSA in PBS), containing 2% goat serum. After being washed three times, cells were incubated for 1 h with affinity-purified rabbit anti-Grp78 polyclonal antibody (1:120 dilution) in the blocking solution. This was followed by incubation with affinity-purified goat anti-rabbit Cy5 F(ab′) fragment (1:150 dilution) at room temperature for 1 h. Cells were imaged by conventional confocal microscopy on a Bio-Rad Radiance 2000 scanning laser system.

RESULTS

*Development of Compound **I**, the Most Potent and Selective PTP1B Inhibitor Reported to Date*. PTP substrate specificity studies have shown that pTyr alone is not sufficient for high-affinity binding and that residues flanking pTyr furnish additional interactions for specific and high-affinity substrate recognition (*23*). These studies, together with the discovery of a second nonconserved aryl phosphate-binding site adjacent to the active site in PTP1B (*24*), suggested a novel paradigm for the creation of potent and specific PTP inhibitors, namely, bidentate ligands designed to bind to both the active site and a unique adjacent peripheral site. Using a combinatorial library/high-throughput screening approach, we have acquired a bidentate PTP1B inhibitor (compound **I**, Figure 1) capable of simultaneously occupying both the active site and a unique peripheral site in PTP1B (*26*−*28*). Mutagenesis and structural analysis of the interactions between PTP1B and **I** revealed that the phosphonodifluoromethylphenylalanine (F_2Pmp) group occupies the active site, the linker Asp forms interactions with residues Arg47 and Asp48, and the distal 4-phosphonodifluoromethylphenylacetyl group makes both van der Waals and ionic contacts with Arg47 and Lys41. Compound **I** is the most potent and selective PTP1B inhibitor identified to date, as it displays a K_i value of 2.4 nM for PTP1B and exhibits selectivity, several orders of magnitude, in favor of PTP1B against a panel of PTPs (*26*). Unfortunately, treatment of a number of cell lines with **I** has no direct effect on insulin signaling, indicating that compound **I** may not be able to penetrate the cell membrane. This is not surprising given

Scheme 1: Solid Phase Peptide Synthesis (Rink resin) of the N-Terminally Fatty Acid-Derivatized PTP1B Inhibitor **II**

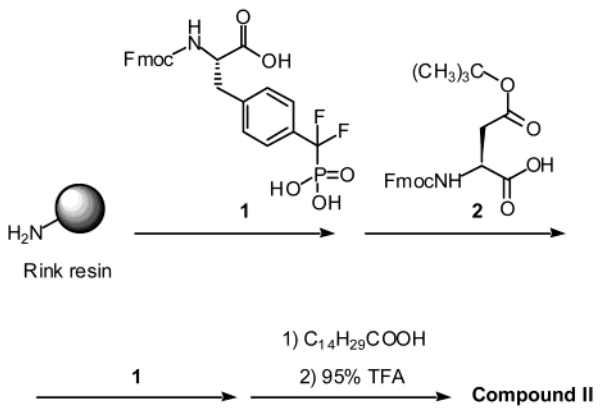

the fact that compound **I** contains five negative charges. To increase cell membrane permeability, we attached a highly lipophilic fatty acid to **I**. This approach has proven to be effective in enabling membrane penetration of a negatively charged trissulfotyrosyl dodecapeptide (*34*).

*Synthesis of Fatty Acid-Derivatized PTP1B Inhibitors **II** and **III***. Two membrane permeable fatty acid-modified derivatives of **I** were prepared. The fatty acid-derivatized species **II** was synthesized on the Rink resin according to the protocol outlined in Scheme 1. Sequential coupling of *N*-Fmoc-4-(difluorophosphonomethyl)-L-phenylalanine **1**, the protected aspartic acid derivative **2**, compound **1**, and pentadecanoic acid followed by side chain deprotection and cleavage from the resin furnished the desired membrane permeable PTP1B inhibitor **II**. We also developed an alternate strategy for incorporating a membrane-permeabilizing alkyl chain element into **I**. The alkoxyl benzaldehyde resin **7** contains an aldehyde functionality that can be used to reductively alkylate a wide assortment of amines, including amino esters (*35*−*37*), aliphatic amines (*38*, *39*), and aromatic amines (*40*). We employed the aldehyde functionality as a handle to introduce the long chain tetradecyl moiety at the C-terminus of the PTP1B inhibitor (**III**). The latter was prepared via a convergent approach in which Cys-containing derivative **6** was coupled to tetradecyl-substituted species **14**. Compound **6** was synthesized on the Rink resin via the sequential addition of *N*-Fmoc-*S*-trityl-L-cysteine **3**, *N*-Fmoc-6-aminohexanoic acid **4**, *N*-Fmoc-4-(difluorophosphonomethyl)-L-phenylalanine **1**, protected aspartic acid derivative **2**, and Fmoc-protected phenylacetic acid derivative **5** (see Experimental Procedures for the synthesis of this compound). Side chain deprotection and cleavage from the resin furnished **6** (Scheme 2). Compound **14** was synthesized on FMPB AM resin **7** (Scheme 3). Reductive alkylation furnished N-substituted resin **8**, which was subsequently acylated with protected lysine derivative **9**. Side chain deprotection, sulfonylation with Lissamine **11**, deprotection of the α-amino moiety of lysine, acylation with ϵ-maleimidocapric acid **12**, and cleavage from the resin provided **14**. Compound **6** was then coupled to **14** to furnish the desired membrane permeable fluorophore-appended PTP1B inhibitor **III**.

*Compounds **II** and **III** Are Potent and Selective Cell Permeable PTP1B Inhibitors*. In addition to the fatty acid tail, compound **II** differs from **I** in that the distal 4-phosphonodifluoromethylphenylacetyl group is replaced with an F_2-Pmp group, which greatly simplifies the synthesis. Like **I**, compound **II** acts as a competitive and reversible PTP1B inhibitor with a K_i value of 26 nM. Despite the decreased affinity, compound **II** displays a selectivity profile similar to that of **I** (data not shown). On the basis of the crystal structure of PTP1B bound with compound **I** (*28*), it is unlikely that the site of fatty acid modification in **II** would have any adverse effect on PTP1B binding. The decreased affinity for **II** is likely due to the extra methylene unit in the distal F_2Pmp group, which may weaken the interaction between PTP1B and the terminal phosphonate group (*26*−*28*).

Although compound **I** is not membrane permeable and exerts no cellular activity, compound **II** is highly effective at blocking PTP1B activity in a number of cell lines (unpublished observations and see below). This is consistent with previous observations that highly lipophilic fatty acids enable membrane penetration of negatively charged compounds. To provide further evidence that the observed cellular effects of **II** are the result of PTP1B inhibition inside the cell, we sought to determine the cellular localization of compound **III** (Figure 1), a derivative of compound **I** containing Rhodamine B and a fatty acid. Compound **III** possesses potency and selectivity for PTP1B similar to those of **II**. Significant uptake of **III** was observed by confocal microscopy in a number of cell lines, including CHO, COS, HepG2, and L6 cells (data not shown), while no fluorescence was observed in cells incubated with Rhodamine B or inhibitor without fatty acid. PTP1B is localized to the cytoplasmic face of the endoplasmic reticulum (ER) through the 35 C-terminal residues (*41*, *42*). To confirm that compound **III** is colocalized with PTP1B, CHO/HIRc cells expressing PTP1B fused with a green fluorescent protein (GFP) were treated with **III** for 1 h. Subsequently, the permeabilized cells were probed with antibodies to Grp78, a known ER marker protein (*43*). We confirmed that PTP1B resides on the ER as shown by its colocalization with Grp78 (Figure 2F). In addition, the merged fluorescence image from PTP1B-GFP and compound **III** (Figure 2C) suggests that a population of **III** binds to PTP1B and is colocalized with PTP1B on the ER.

Having achieved bioavailability and at the same time maintained low nanomolar potency for compound **II**, we carried out our subsequent biological studies with **II**. In the following, we describe the effects of compound **II** on both metabolic and mitogenic pathways stimulated by insulin in both intact CHO/HIRc cells and L6 myotubes.

*Compound **II** Increases the Extent of IRβ and IRS-1 Tyrosine Phosphorylation in CHO/HIRc Cells*. CHO/HIRc cells were incubated with a range of concentrations of **II** (0 nM, 50 nM, 125 nM, 1.25 μM, and 12.5 μM) for 1 h, which was followed by treatment with or without 10 nM insulin for 5 min (Figure 3). DMSO (0.1%, lane 1) and sodium vanadate (1 mM, lane 11) were used as negative and positive controls, respectively. The cell lysates were subjected to SDS−PAGE, transferred to nitrocellulose membrane, and followed by Western blot with anti-pTyr antibodies. As shown in Figure 3, compound **II** can synergistically increase the insulin-induced tyrosine phosphorylation levels of both IRβ and IRS-1. The maximal effect of **II** in CHO/HIRc cells seems to peak between 125 nM and 1.25 μM. At a higher compound **II** concentration (i.e., 12.5 μM, ∼500 times its

Scheme 2: Solid Phase Peptide Synthesis (Rink resin) of Cysteine-Containing Precursor **6** to PTP1B Inhibitor **III**

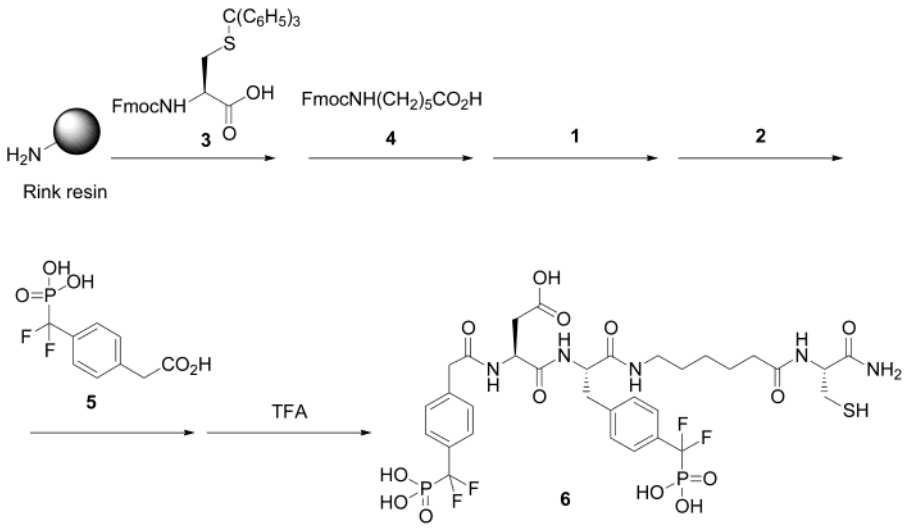

Scheme 3: Solid Phase Synthesis (FMPB AM resin) of Rhodamine-, Tetradecyl-, and Maleimide-Substituted Precursor **14** to PTP1B Inhibitor **III**

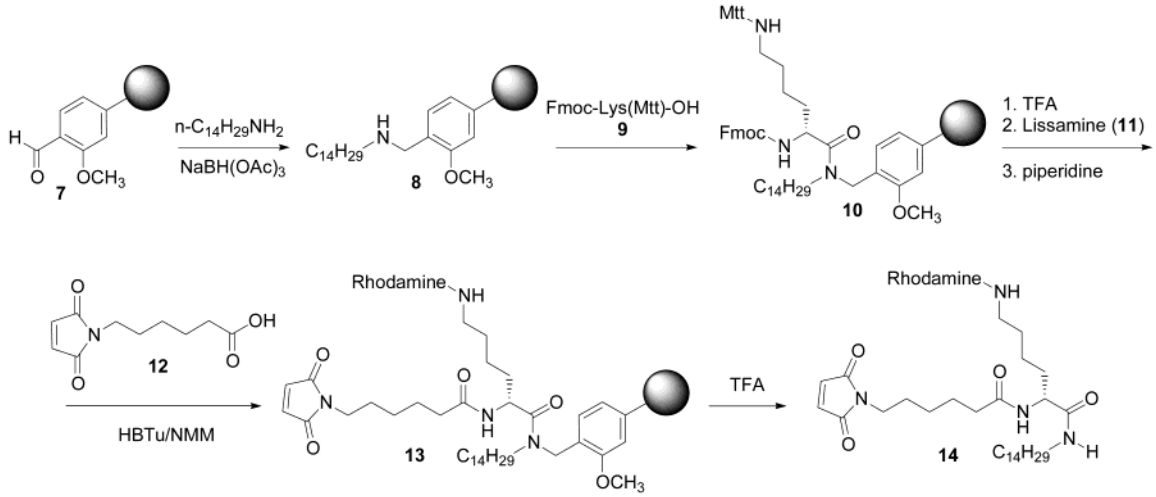

K_i value), the phosphorylation levels of IRβ and IRS-1 actually decrease, which may be caused by nonspecific effects. It is of interest to note that treatment with vanadate, a nonspecific PTP inhibitor, does not lead to an increased level of tyrosine phosphorylation of IRS-1. To determine the effect of **II** on IRβ and IRS-1 phosphorylation in the absence of insulin, anti-pTyr Western blots were performed with immunocomplexes of anti-IRβ and anti-IRS-1 antibodies. When normalized against the IRβ and IRS-1 protein levels, the results showed that treatment of cells with compound **II** alone increased the basal tyrosine phosphorylation levels of both IRβ and IRS-1 (data not shown). In fact, the basal pTyr level of IRβ increased 53, 159, and 320% while that of IRS-1 increased 19, 43, and 128% when cells were treated with 125 nM, 500 nM, and 1.25 μM **II**, respectively.

*Compound **II** Activates both Akt and ERK1/2 in CHO/HIRc Cells*. To study the effect of **II** on insulin signaling downstream of IRβ and IRS-1, CHO/HIRc cells pretreated with 125 nM **II** for various time intervals were stimulated with or without 10 nM insulin. Activated Akt and ERK1/2 were detected using phospho-specific Akt and ERK1/2 antibodies. As shown in Figure 4, the stimulating effect of **II** peaked at 4 h, at which time compound **II** potentiated the insulin-stimulated Akt and ERK1/2 phosphorylation by 59 and 42%, respectively. In addition, compound **II** alone also increased the basal level of phosphorylation of Akt and ERK1/2 3.3- and 2.2-fold, respectively. Thus, consistent with the effect seen on the phosphorylation of IRβ and IRS-1, compound **II** is capable of augmenting the insulin-induced Akt and ERK1/2 activation, as well as activating both Akt and ERK1/2 in the absence of insulin.

*Compound **II** Enhances Glucose Uptake, Elk1 Phosphorylation, and Cell Proliferation in CHO/HIRc Cells*. To further evaluate the biological consequences of the compound **II**-stimulated increase in the level of IRβ and IRS-1 phosphorylation as well as Akt and ERK1/2 activity, the ability of compound **II** to mimic insulin in promoting glucose uptake, gene transcription, and cell proliferation was assessed. Since Akt is essential for the insulin-stimulated Glut4 translocation to the plasma membrane, agents that increase Akt activity should enhance cellular glucose uptake. Indeed, as shown in Figure 5A, CHO/HIRc cells treated with **II** for 1 h displayed a concentration-dependent increase in the rate of glucose uptake when compared to the untreated controls. Thus, the rate of basal glucose uptake increased by 18, 31, 68, and 78% in the presence of 50 nM, 125 nM, 500 nM,

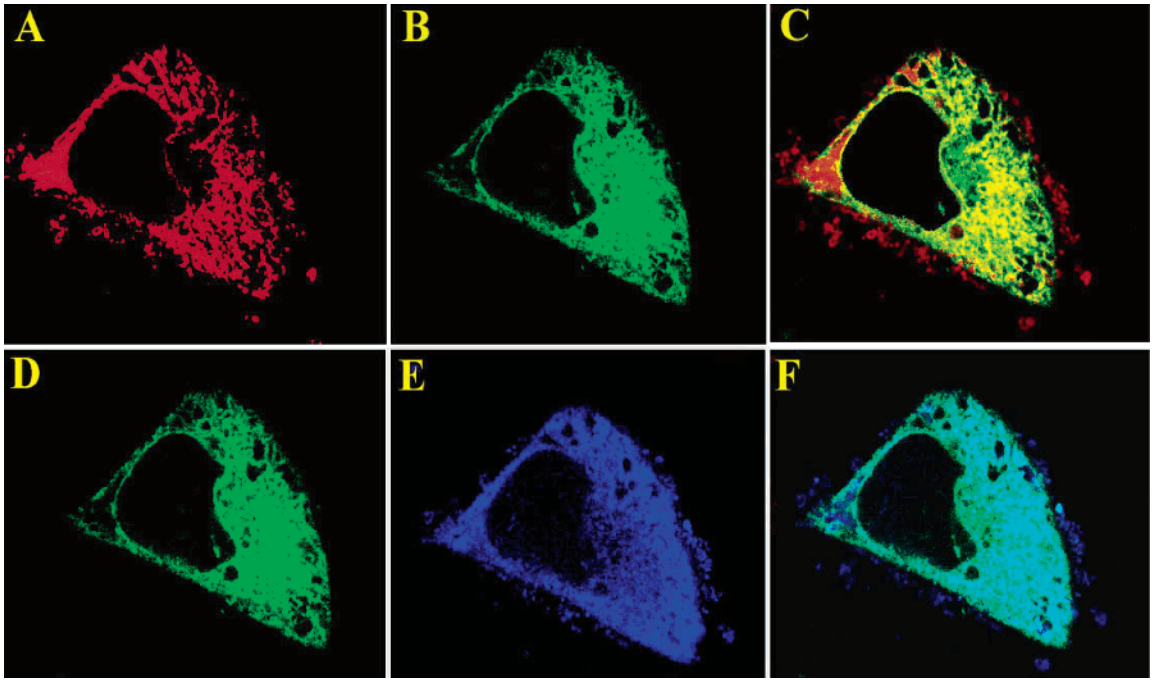

FIGURE 2: Colocalization of PTP1B and compound **III** on ER in CHO/HIRc cells. CHO/HIRc cells transfected with a plasmid expressing full-length PTP1B conjugated to green fluorescence protein were treated with **III** for 1 h. After fixation and permeabilization, cells were costained with rabbit anti-Grp78 polyclonal antibody and goat anti-rabbit Cy5 F(ab′)2 fragment. Panels A and B are the fluorescence images of rhodamine from **III** (red) and PTP1B-GFP (green), respectively. Panel C is the superimposition of panels A and B (yellow) of the same cell. Panels D and E are the fluorescence images of PTP1B-GFP (green) and GRP78/Bip (blue), respectively, and panel F is the superimposition of panels D and E (light blue) of the same cell.

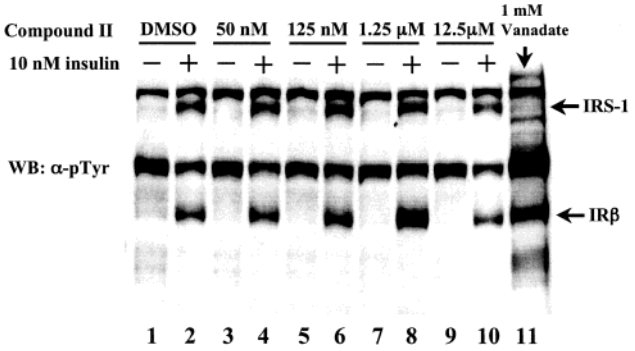

FIGURE 3: Effect of **II** and insulin on tyrosine phosphorylation of IRβ and IRS-1 in CHO/HIRc cells. Subconfluent CHO/HIRc cells were incubated with a range of concentrations of **II** (0 nM, 50 nM, 125 nM, 1.25 μM, and 12.5 μM) for 1 h, followed by a 5 min treatment with (lanes 2, 4, 6, 8, and 10) or without (lanes 1, 3, 5, 7, and 9) 10 nM insulin. The cell lysates (50 μg of proteins) were subjected to SDS−PAGE and the resolved polypeptides transferred to nitrocellulose membranes, which were blocked with anti-pTyr antibodies. The identity of IRβ and IRS-1 was confirmed by stripping the membrane and reprobing it with anti-IRβ and anti-IRS-1 antibodies.

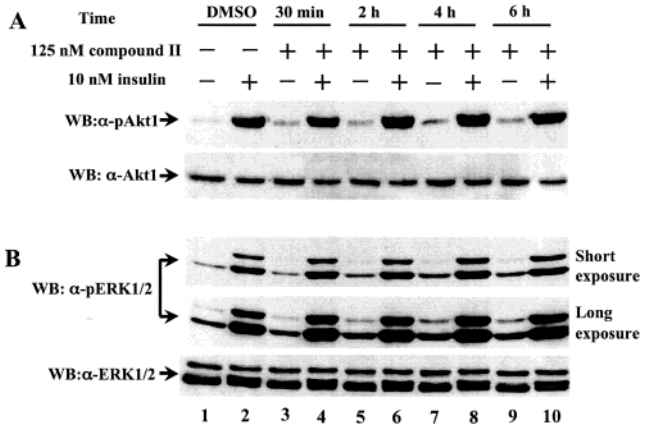

FIGURE 4: Effect of **II** on Akt and ERK1/2 phosphorylation in CHO/HIRc cells. CHO/HIRc cells were treated with 125 nM **II** in 0.1% DMSO for various amounts of time. Subsequently, the cells were stimulated without (lanes 1, 3, 5, 7, and 9) or with (lanes 2, 4, 6, 8, and 10) 10 nM insulin for 5 min. Total cell lysates (50 μg of protein) were subjected to SDS−PAGE, transferred to nitrocellulose membranes, and immunoblotted with either phospho-specific Akt or phospho-specific ERK1/2 antibodies.

and 1.25 μM compound **II**, respectively. In addition, incubation of CHO/HIRc cells with **II** (500 nM for 1 h) also augmented insulin-stimulated glucose uptake by 50% at a submaximal insulin concentration (0.0001 nM), while the same treatment had no significant effect at saturating insulin concentrations (0.01−0.1 nM) (Figure 5B).

To further corroborate the observation that compound **II** has a positive effect on the ERK1/2 pathway, we assessed the activation of transcription factor Elk1, a direct downstream substrate of ERK1/2, in CHO/HIRc cells transiently cotransfected with an Elk1 expression vector and the pFR-Luc plasmid that contains a luciferase reporter gene. When activated by phosphorylation, the Elk1 fusion protein binds to the promoter and induces luciferase expression. After cotransfection and serum starvation for 4 h, the cells were incubated with or without 10 nM insulin in the presence of different concentrations of compound **II** for 30 h. As shown in Figure 6A, compound **II** increases luciferase activity (which is a direct measure of ERK1/2 activity on Elk1) either alone or in combination with insulin in a dose-dependent manner. We also measured the mitogenic response of CHO/HIRc cells exposed to **II**. In these experiments, cells were incubated with different concentrations of **II** with or without 10 nM insulin for 48 h in the presence of 2% FBS. An

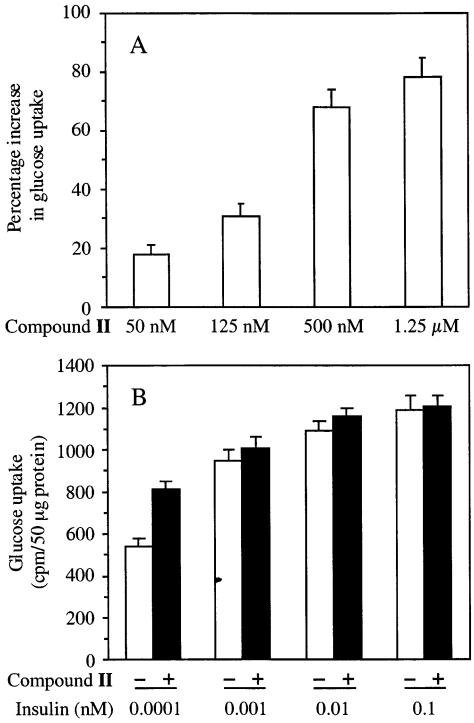

FIGURE 5: Effect of **II** on 2-deoxyglucose uptake in CHO/HIRc cells. CHO/HIRc cells were serum starved for 3−4 h and then incubated with a range of **II** concentrations (50 nM, 125 nM, 500 nM, and 1.25 μM) in KRP buffer for 1 h (A) or incubated with 500 nM **II** for 1 h followed by stimulation with a range of insulin concentrations for 30 min (B). The rate of glucose uptake was measured following the addition of 2-deoxy[1,2-^{3}H]glucose at 37 °C for 1 min. The rate of glucose uptake is expressed as the percentage of the basal value of cells treated with 0.1% DMSO. The graph shows the means ± standard error (SE) of at least three experiments.

increased level of proliferation was observed in cells treated with compound **II** either alone or in combination with insulin (Figure 6B). Together, these data are consistent with the fact that compound **II** both mimics and potentiates insulin-induced ERK1/2 activation.

*Compound **II** Exerts Its Effect Upstream of PI3K and MEK1*. Since compound **II** appears to affect both PI3K and ERK1/2 pathways, we sought to determine whether **II** exerts its effect up- or downstream of PI3K or MEK1. In one set of experiments, CHO/HIRc cells were exposed to either 100 nM wortmannin, a small molecule PI3K inhibitor (*44*, *45*), or 4 μM U0126, a small molecule MEK1 inhibitor that is capable of blocking ERK1/2 activation (*46*), for 30 min, which was followed by treatment with 125 nM **II** for 4 h. The cells were subsequently stimulated with or without 10 nM insulin for 5 min. In another set of experiments, the cells were incubated with 125 nM **II** for 3.5 h followed by a 30 min treatment with either 100 nM wortmannin or 4 μM U0126 prior to a 5 min stimulation with or without 10 nM insulin. As expected, neither wortmannin nor U0126 affected IRβ or IRS-1 tyrosine phosphorylation (data not shown). Interestingly, wortmannin blocked Akt1 activation induced either by **II** alone or in combination with insulin (Figure 7A), suggesting that PTP1B probably functions upstream of PI3K in the insulin signal pathways. Similarly, U0126 blocked ERK1/2 activation induced either by **II** alone or in combination with insulin (Figure 7B), indicating that PTP1B may regulate the insulin-stimulated ERK1/2 pathway at a step upstream of MEK1. We note that when cells were pretreated with PIK3 or MEK1 inhibitors before the 4 h incubation with **II**, the observed blockage of Akt or ERK1/2 activation was not as impressive as that seen in experiments in which the PIK3 or MEK1 inhibitors were added after the cells were treated with compound **II** for 3.5 h (Figure 7). One potential explanation for this may relate to the *in vivo* stabilities of wortmannin and U0126. Taken together, the pharmacological studies suggest that the most likely substrates for PTP1B are IRβ and IRS-1, although the possibility exists that the observed increase in the level of IRS-1 phosphorylation is not a direct result of PTP1B inhibition but rather an indirect result of increased IRβ phosphorylation and/or activity.

*Effects of Compound **II** on Akt and ERK1/2 Activation in L6 Myotubes*. We next tested the effects of compound **II** on Akt and ERK1/2 activation in more physiologically relevant cells, the differentiated L6 myotubes. In this experiment, cells were treated for 1 h with several concentrations of **II** followed by a brief stimulation (5 min) with or without insulin (50 nM). As shown in Figure 8, treatment with compound **II** increased the level of basal Akt phosphorylation as well as the insulin-stimulated Akt phosphorylation in a concentration-dependent manner. Thus, the level of basal Akt phosphorylation in L6 myotubes was increased 2.4-, 2.9-, 4.5-, and 3.5-fold by incubation with 50 nM, 125 nM, 500 nM, and 1.25 μM compound **II**, respectively. In addition, the insulin-induced Akt phosphorylation was enhanced by 52, 63, 66, and 56% by compound **II** at concentrations of 50 nM, 125 nM, 500 nM, and 1.25 μM, respectively. As expected, unlike the results obtained from CHO/HIRc cells, compound **II** had no measurable effect on ERK1/2 phosphorylation in L6 myotubes (data not shown).

*Compound **II** Enhances Glucose Uptake in L6 Myotubes*. Finally, we measured the effect of compound **II** on glucose uptake in L6 myotubes both in the absence and in the presence of a range of insulin concentrations. In the absence of insulin, the rate of basal glucose uptake increased by 53, 70, and 92% at 50 nM, 125 nM, and 1.25 μM compound **II**, respectively (incubation for 1 h) (Figure 9A). To determine the effect of compound **II** on the insulin dose−response curve, L6 myotubes were treated with 125 nM **II** (1 h) and stimulated with a range of insulin concentrations for 30 min. As shown in Figure 9B, the insulin dose−response curve for insulin-induced glucose uptake was shifted to the left in the presence of compound **II**. The EC_{50} value decreased from 6.4 nM in the absence of **II** to 1.4 nM in the presence of 125 nM **II**, resulting in a 4.6-fold increase in insulin sensitivity. Moreover, compound **II** (125 nM) approximately doubled the rate of glucose uptake at a submaximal insulin concentration (0.1 nM), while at maximal insulin concentrations (25−100 nM), compound **II** no longer had an effect. Thus, inhibition of PTP1B enhances the potency but not the efficacy of insulin in glucose transport.

DISCUSSION

Protein tyrosine phosphorylation is essential for the regulation of many important cellular processes (*47*). To varying degrees, many diseases are characterized by either excessive or diminished signaling involving tyrosine phosphorylation. Type 2 diabetes is associated with insulin

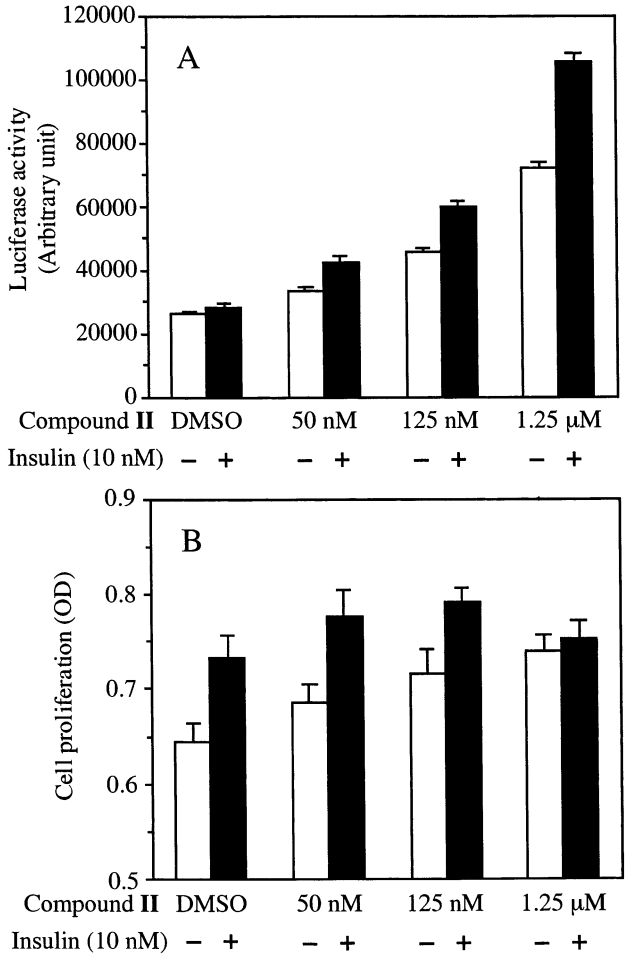

FIGURE 6: Effects of **II** on the ERK1/2 pathway. (A) Effect of **II** on Elk1 phosphorylation in CHO/HIRc cells. CHO/Hirc cells were cotransfected with the fusion transactivator plasmid (pFA-Elk1) and the reporter plasmid (pFR-Luc) as well as pCMV-β-gal as described in Experimental Procedures. Twenty-four hours after transfection, the cells were incubated with the indicated concentrations of **II** or combined with 10 nM insulin for 30 h. The extent of Elk-1 activation is expressed by the luciferase activity. (B) Effect of **II** on proliferation of CHO/HIRc cells. Cells were incubated with a range of concentrations of **II** together with or without 10 nM insulin for 48 h in the presence of 2% FBS. The MTS tetrazolium compound (Owen's reagent) was added to the cells and incubated for 1 h at 37 °C, and the absorbance at 490 nm was measured.

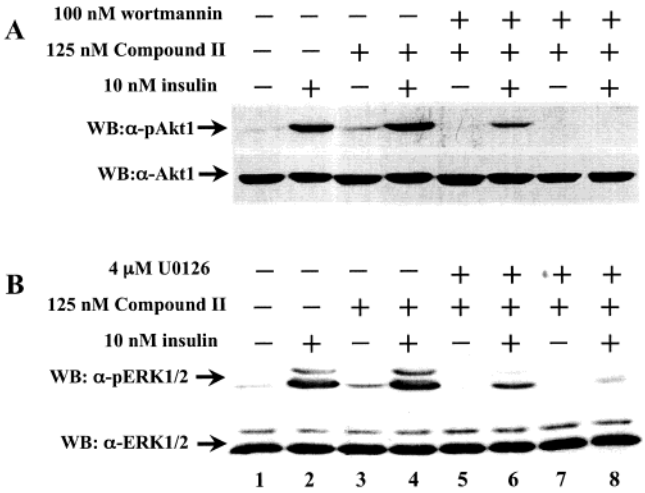

FIGURE 7: Compound **II** exerts its effect upstream of PI3K and MEK1. CHO/HIRc cells were exposed to either 100 nM wortmannin (A) or 4 μM U0126 (B) for 30 min followed by treatment with 125 nM **II** for 4 h (lanes 5 and 6). Subsequently, the cells were stimulated with or without 10 nM insulin for 5 min. Alternatively, the cells were incubated with 125 nM **II** for 3.5 h followed by a 30 min treatment with either 100 nM wortmannin (A) or 4 μM U0126 (B) prior to a 5 min stimulation with or without 10 nM insulin (lanes 7 and 8). For controls, cells were treated with either 0.1% DMSO (lanes 1 and 2) or 125 nM **II** (lanes 3 and 4) for 4 h, followed by treatment with (lanes 2 and 4) or without (lanes 1 and 3) 10 nM insulin for 5 min. Cell lysates (50 μg) were subjected to SDS−PAGE and immunoblotted with either anti-phospho-specific Akt and anti-Akt antibodies (A) or anti-phospho-specific ERK1/2 and anti-ERK1/2 antibodies (B).

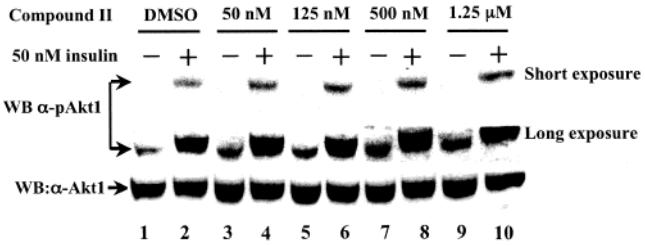

FIGURE 8: Effect of **II** on Akt phosphorylation in L6 myotubes. Differentiated L6 myotubes were treated with different concentrations of **II** for 1 h, followed by stimulation with or without 50 nM insulin for 5 min. Total cell lysates (50 μg) were resolved by SDS−PAGE and subjected to anti-phospho-specific Akt and anti-Akt immunoblotting.

resistance, possibly due to attenuated signaling from the receptor molecule. At the cellular level, insulin resistance is manifested as either reduced capacity (diminished response to a maximum amount of insulin) or reduced sensitivity (a rightward shift in the insulin dose−response curve) to promote glucose transport and metabolism (*48*). Although the molecular defect(s) responsible for insulin resistance remains unknown, most evidence suggests that it may involve early steps in insulin signal transduction. Since termination of insulin signaling requires the dephosphorylation of IRβ and its downstream effector molecules, it was hypothesized that dysregulation of PTPs, through increased activity or expression, can attenuate insulin signaling resulting in insulin resistance. Theoretically, thwarting the action of PTPs that terminate insulin signaling would be expected to increase insulin sensitivity.

As summarized in the introductory section, there is substantial evidence from overexpression, knockout, and antisense experiments (*12*−*22*) implicating PTP1B as a major negative regulator of insulin signaling. However, results from small molecule PTP1B inhibitors are limited. Pharmacological studies of potent and specific PTP1B inhibitors are important for the eventual validation of this enzyme as a therapeutic target. To further define the role of PTP1B in insulin-stimulated signal pathways, and to test the hypothesis that blocking the activity of PTP1B would augment and prolong the action of insulin, we have carried out a number of experiments to assess the cellular effects of potent and selective synthetic PTP1B inhibitors on insulin signaling in several insulin sensitive cell lines. Since compound **I** failed to penetrate cells, we decided to make fatty acid analogues **II** and **III**. Fatty acid-modified **II** and **III** achieved bioavailability and remained as nanomolar PTP1B inhibitors. Consequently, we have carried out detailed analyses of the effects of compound **II** on both the metabolic and mitogenic pathways stimulated by insulin in both CHO/HIRc cells and L6 myotubes.

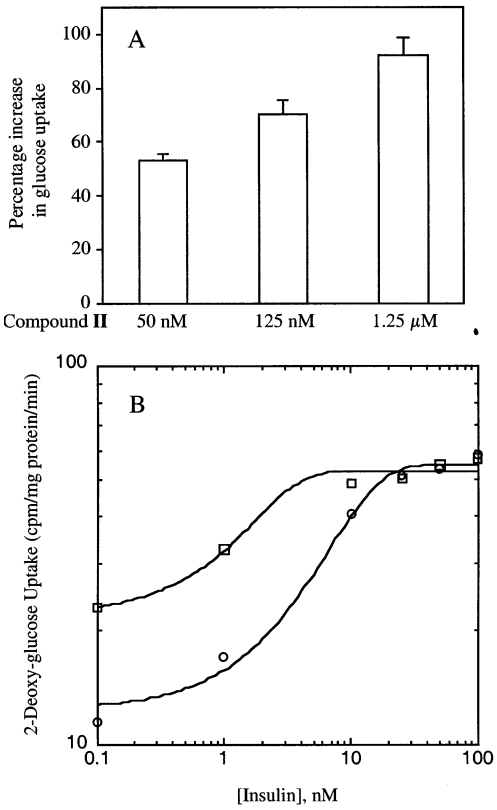

FIGURE 9: Effect of compound **II** on glucose uptake in L6 myotubes. Differentiated L6 myotubes were serum starved for 5 h. Subsequently, the cells were treated with a range of concentrations of compound **II** for 1 h in the absence of insulin (A). Alternatively, the cells were treated with 125 nM **II** (□) or without **II** (○) for 1 h followed by stimulation with a range of insulin concentrations for 30 min (B). The rate of glucose uptake was measured at 37 °C for 3 min followed by the addition of 2-deoxy-[1,2-^{3}H]glucose to a Hepes-buffered saline solution. In panel A, the rate of glucose uptake is expressed as the percentage of the basal value of the cells treated with 0.1% DMSO. The graph shows the means ± SE of four to six experiments. In panel B, the rate of glucose uptake is expressed as the absolute value normalized vs the protein level.

In CHO/HIRc cells, blocking PTP1B activity with compound **II** synergistically enhanced the insulin-stimulated IRβ and IRS-1 phosphorylation (Figure 3), Akt and ERK1/2 activation (Figure 4), glucose uptake (Figure 5), and Elk1 transcriptional activation and cell proliferation (Figure 6). Moreover, compound **II** alone also substantially increased the level of basal phosphorylation in IRβ, IRS-1, Akt, and ERK1/2 (Figures 3 and 4), as well as the levels of glucose uptake, Elk1 activation, and proliferation (Figures 5 and 6). Pharmacological studies with wortmannin and U0126 in combination with **II** (Figure 7) suggest that PTP1B exerts its negative effect on insulin signaling upstream of PI3K and MEK1, most likely by directly dephosphorylating both IRβ and IRS-1. This is consistent with previous observations implicating IRβ and IRS-1 as direct substrates of PTP1B (*12*−*17*, *21*, *22*).

We also determined the effect of blocking PTP1B activity in L6 myotubes. Consistent with results obtained with CHO/HIRc cells, treatment of L6 myotubes with compound **II** not only augmented the insulin-stimulated Akt phosphorylation but also increased the basal level of Akt phosphorylation (Figure 8). As expected, in the absence of insulin, compound **II** also boosted basal glucose uptake in a concentration-dependent manner. In addition, incubation of L6 myotubes with 125 nM (5 times its K_i value) **II** also resulted in a leftward shift in the insulin dose−response curve, causing a 4.6-fold increase in insulin sensitivity for glucose uptake (Figure 9). The observed cellular effects of compound **II** are likely due to direct inhibition of PTP1B activity, since **II** does not affect general tyrosine phosphorylation in PTP1B knockout cells (A. Cheng and M. Tremblay, personal communication). Finally, we also found that a previously identified small molecule PTP1B inhibitor (compound **33** in ref *25*) not only potentiated the insulin-induced IRβ phosphorylation but also increased its basal level of phosphorylation in baby hamster kidney cells expressing the human insulin receptor. In addition, this compound also increased the rate of Glut4 translocation to the plasma membrane both in the absence and in the presence of insulin in 3T3-L1 adipocytes (data not shown).

Collectively, our pharmacological studies demonstrate that potent and selective small molecule PTP1B inhibitors can increase the level of both basal and insulin-stimulated receptor signaling. Thus, our data indicate that small molecule inhibitors targeted to PTP1B can act as both insulin mimetics and sensitizers, which enable a greater response for a given amount of insulin. The insulin mimetic effect of PTP1B inhibitors is a novel finding because previous PTP1B knockout and antisense studies did not indicate such an effect from a decrease in PTP1B activity. The insulin mimetic effect of PTP1B inhibitors likely results from an increase in the IRβ phosphorylation level in the resting state. This corroborates the idea that the overall state of IRβ phosphorylation in quiescent cells is the net result of basal IR kinase and PTP activities. The insulin sensitizing effect of PTP1B inhibitors may arise from a reduction in the rate of dephosphorylation of the activated receptor.

Recent imaging studies suggest that PTP1B-catalyzed dephosphorylation requires endocytosis of the receptors and occurs at specific sites on the surface of the ER (*49*). We showed by immunofluorescence confocal microscopy that a rhodamine-labeled PTP1B inhibitor (compound **III**) binds to and colocalizes with the GFP-labeled PTP1B on ER in CHO/HIRc cells (Figure 2). It is interesting to note that, in general, PTP1B inhibitors exert a greater effect on basal rather than insulin-stimulated IR signaling. This suggests that ER-anchored PTP1B may play a major role in keeping the internalized or newly synthesized insulin receptors in the unphosphorylated states. Since the IRβ tyrosine kinase is not entirely quiescent and PTP1B may be required to dampen spontaneous phosphorylation, inhibition of PTP1B activity would be expected to increase the basal level of IRβ phosphorylation.

It is likely that PTP1B is not the only PTP that downregulates insulin signaling. Other PTPs (e.g., LAR and PTPα) (*50*−*52*), in addition to PTP1B, may function at the plasma membrane to deactivate the IR. Consistent with this notion is the fact that deletion of the PTP1B gene in mice decreases but does not abolish the rate of dephosphorylation of IRβ and IRS-1 (*21*). Indeed, in PTP1B knockout mice, IRβ phosphorylation in the liver is prolonged only 2-fold, while in the muscle, the rate of IRβ phosphorylation increased only 2-fold. Although the effects may seem small, PTP1B$^{-/-}$ mice are resistant to diabetes and obesity (*21*, *22*). In light of these findings, the observed cellular effects with compound **II** are

highly significant (Figures 3−8). These effects include a 2−3-fold increase in the levels of IRβ and IRS1 phosphorylation, Akt activation in the absence of insulin, and up to 60−90% augmentation in IRβ and IRS1 phosphorylation, and Akt activation in the presence of insulin when the cells are treated with 125 nM compound **II** (5 times its K_i value). In addition, the rate of basal glucose uptake of L6 myotubes increased by 70% in the presence of 125 nM compound **II** (Figure 9A), and incubation of L6 myotubes with 125 nM **II** also resulted in a leftward shift in the insulin dose−response curve, causing a 4.6-fold increase in insulin sensitivity for glucose uptake (Figure 9B). Collectively, the observed cellular effects of compound **II** are in line with what should be expected from the PTP1B knockout model.

Our study also establishes the utility of potent and selective PTP1B inhibitors in further studies of the roles of PTP1B in other signal pathways. In addition to a role in insulin signaling, PTP1B is also implicated in several other physiological and pathological processes, including leptin-stimulated pathways (*53*, *54*), transformation by the *Neu* oncogene (*55*), Src kinase activation (*56*), antagonizing signaling by the EGF receptor (*57*, *58*) and the oncoprotein $p210^{bcr-abl}$ (*59*), the negative regulation of cadherin-mediated adhesion and signaling via its association with cadherin and dephosphorylation of β-catenin (*60*), and the negative regulation of integrin-mediated signaling by binding to and possibly dephosphorylating $p130^{cas}$ (Crk-associated substrate) (*61*). Potent and selective PTP1B inhibitors characterized in this study should be extremely useful in helping to rapidly establish the precise functions for PTP1B, both in normal cellular physiology and under pathogenic conditions. The pharmacological approach is advantageous over classical genetic analyses because of its simplicity, speed, tunability, and reversibility. In addition, small molecule inhibitors and/or activators exert their effect on endogenous targets, avoiding the need for overexpression of dominant-negative or constitutively active mutants, which can cause artifacts and lead to erroneous conclusions. Indeed, the availability of agents with specificity for a particular kinase has greatly enhanced our ability to identify its substrates and physiological functions. This study demonstrates that pharmacological investigation of PTPs with specific inhibitors will be equally as informative.

In conclusion, we have described a comprehensive evaluation of a highly selective and potent PTP1B inhibitor in a number of cell lines. We note that the observed cellular effects for compound **II** are the most pronounced among all reported studies for insulin sensitizing agents. Although gene knockout and overexpression studies have implicated a negative role of PTP1B in insulin signaling, results presented in this study provide the much-needed direct validation that small molecule inhibitors targeted to PTP1B will be beneficial for type II diabetes. In addition, we have shown that PTP1B inhibitors are not only insulin sensitizers (as expected from PTP1B knockout data) but also insulin mimetics. The latter is a novel finding and was not apparent from the knockout study. Taken together, our findings, combined with results from PTP1B knockout and biochemical studies, provide strong evidence that PTP1B negatively regulates insulin signaling and that small molecule PTP1B inhibitors have the ability to potentiate and mimic the action of insulin.

REFERENCES

1. White, M. F., and Kahn, C. R. (1994) *J. Biol. Chem. 269*, 1−4.
2. Avruch, J. (1998) *Mol. Cell. Biochem. 182*, 31−48.
3. White, M. F. (1998) *Mol. Cell. Biochem. 182*, 3−11.
4. Saltiel, A. R., and Kahn, C. R. (2001) *Nature 414*, 799−806.
5. Ruderman, N. B., Kapeller, R., White, M. F., and Cantley, L. C. (1990) *Proc. Natl. Acad. Sci. U.S.A. 87*, 1411−1415.
6. Cheatham, B., Vlahos, C. J., Cheatham, L., Wang, L., Blenis, J., and Kahn, C. R. (1994) *Mol. Cell. Biol. 14*, 4902−4911.
7. Downward, J. (1998) *Curr. Opin. Cell Biol. 10*, 262−267.
8. Czech, M. P., and Corvera, S. (1999) *J. Biol. Chem. 274*, 1865−1868.
9. Summers, S. A., Yin, V. P., Whiteman, E. L., Garza, L. A., Cho, H., Tuttle, R. L., and Birnbaum, M. J. (1999) *Ann. N.Y. Acad. Sci. 892*, 169−186.
10. Holman, G. D., and Kasuga, M. (1997) *Diabetologia 40*, 991−1003.
11. Zhang, Z.-Y. (2001) *Curr. Opin. Chem. Biol. 5*, 416−423.
12. Kenner, K. A., Anyanwu, E., Olefsky, J. M., and Kusari, J. (1996) *J. Biol. Chem. 271*, 19810−19816.
13. Bandyopadhyay, D., Kusari, A., Kenner, K. A., Liu, F., Chernoff, J., Gustafson, T. A., and Kusari, J. (1997) *J. Biol. Chem. 272*, 1639−1645.
14. Walchli, S., Curchod, M. L., Gobert, R. P., Arkinstall, S., and van Huijsduijnen, H. R. (2000) *J. Biol. Chem. 275*, 9792−9796.
15. Dadke, S., Kusari, J., and Chernoff, J. (2000) *J. Biol. Chem. 275*, 23642−23647.
16. Goldstein, B. J., Bittner-Kowalczyk, A., White, M. F., and Harbeck, M. (2000) *J. Biol. Chem. 275*, 4283−4289.
17. Calera, M. R., Vallega, G., and Pilch, P. F. (2000) *J. Biol. Chem. 275*, 6308−6312.
18. Ahmad, F., Li, P. M., Meyerovitch, J., and Goldstein, B. J. (1995) *Biol. Chem. 270*, 20503−20508.
19. Byon, J. C. H., Kusari, A. B., and Kusari, J. (1998) *Mol. Cell. Biochem. 182*, 101−198.
20. Zinker, B. A., Rondinone, C. M., Trevillyan, J. M., Gum, R. J., Clampit, J. E., Waring, J. F., Xie, N., Wilcox, D., Jacobson, P., Frost, L., Kroeger, P. E., Reilly, R. M., Koterski, S., Opgenorth, T. J., Ulrich, R. G., Crosby, S., Butler, M., Murray, S. F., McKay, R. A., Bhanot, S., Monia, B. P., and Jirousek, M. R. (2002) *Proc. Natl. Acad. Sci. U.S.A. 99*, 11357−11362.
21. Elchebly, M., Payette, P., Michaliszyn, E., Cromlish, W., Collins, S., Loy, A. L., Normandin, D., Cheng, A., Himms-Hagen, J., Chan, C. C., Ramachandran, C., Gresser, M. J., Tremblay, M. L., and Kennedy, B. P. (1999) *Science 283*, 1544−1548.
22. Klaman, L. D., Boss, O., Peroni, O. D., Kim, J. K., Martino, J. L., Zabolotny, J. M., Moghal, N., Lubkin, M., Kim, Y. B., Sharpe, A. H., Stricker-Krongrad, A., Shulman, G. I., Neel, B. G., and Kahn, B. B. (2000) *Mol. Cell. Biol. 20*, 5479−5489.
23. Zhang, Z.-Y. (2002) *Annu. Rev. Pharmacol. Toxicol. 42*, 209−234.
24. Puius, Y. A., Zhao, Y., Sullivan, M., Lawrence, D. S., Almo, S. C., and Zhang, Z.-Y. (1997) *Proc. Natl. Acad. Sci. U.S.A. 94*, 13420−13425.
25. Taing, M., Keng, Y. F., Shen, K., Wu, L., Lawrence, D. S., and Zhang, Z.-Y. (1999) *Biochemistry 38*, 3793−3803.
26. Shen, K., Keng, Y.-F., Wu, L., Guo, X.-L., Lawrence, D. S., and Zhang, Z.-Y. (2001) *J. Biol. Chem. 276*, 47311−47319.
27. Guo, X.-L., Shen, K., Wang, F., Lawrence, D. S., and Zhang, Z.-Y. (2002) *J. Biol. Chem. 277*, 41014−41022.
28. Sun, J.-P., Fedorov, A. A., Lee, S.-Y., Guo, X.-L., Shen, K., Lawrence, D. S., Almo, S. C., and Zhang, Z.-Y. (2003) *J. Biol. Chem. 278*, 12406−12414.
29. Solas, D., Hale, R. L., and Patel, D. V. (1996) *J. Org. Chem. 61*, 1537−1539.
30. Fujishiro, M., Gotoh, Y., Katagiri, H., Sakoda, H., Ogihara, T., Anai, M., Onishi, Y., Ono, H., Funaki, M., Inukai, K., Fukushima, Y., Kikuchi, M., Oka, Y., and Asano, T. (2001) *J. Biol. Chem. 276*, 19800−19806.
31. Asano, T., Shibasaki, Y., Ohno, S., Taira, H., Lin, J. L., Kasuga, M., Kanazawa, Y., Akanuma, Y., Takaku, F., and Oka, Y. (1989) *J. Biol. Chem. 264*, 3416−3420.
32. Asano, T., Katagiri, H., Takata, K., Tsukuda, K., Lin, J. L., Ishihara, H., Inukai, K., Hirano, H., Yazaki, Y., and Oka, Y. (1992) *Biochem. J. 288*, 189−193.
33. Yonemitsu, S., Nishimura, H., Shintani, M., Inoue, R., Yamamoto, Y., Masuzaki, H., Ogawa, Y., Hosoda, K., Inoue, G., Hayashi, T., and Nakao, K. (2001) *Diabetes 50*, 1093−1101.

34. Liotta, A. S., Kole, H. K., Fales, H. M., Roth, J., and Bernier, M. (1994) *J. Biol. Chem. 269*, 22996−23001.
35. Bilodeau, M. T., and Cunningham, A. M. (1998) *J. Org. Chem. 63*, 2800−2801.
36. Boojamra, C. G., Burow, K. M., Thompson, L. A., and Ellman, J. A. (1997) *J. Org. Chem. 62*, 1240−1256.
37. Jensen, K. J., Alsina, J., Songster, M. F., Vagner, J., Albericio, F., and Barany, G. (1998) *J. Am. Chem. Soc. 120*, 5441−5452.
38. Swayze, E. E. (1997) *Tetrahedron Lett. 49*, 8465−8468.
39. Tumelty, D., Schwarz, M. K., Cao, K., and Needels, M. C. (1999) *Tetrahedron Lett. 40*, 6185−6188.
40. Gray, N. S., Kwon, S., and Schultz, P. G. (1997) *Tetrahedron Lett. 38*, 1161−1164.
41. Frangioni, J. V., Beahm, P. H., Shifrin, V., Jost, C. A., and Neel, B. G. (1992) *Cell 68*, 545−560.
42. Woodford-Thomas, T. A., Rhodes, J. D., and Dixon, J. E. (1992) *J. Cell Biol. 117*, 401−414.
43. Baqui, M. M., Gereben, B., Harney, J. W., Larsen, P. R., and Bianco, A. C. (2000) *Endocrinology 141*, 4309−4312.
44. Cantley, L. C., Auger, K. R., Carpenter, C., Duckworth, B., Graziani, A., Kapeller, R., and Soltoff, S. (1991) *Cell 64*, 281−302.
45. Hausdorff, S. F., Fingar, D. C., Morioka, K., Garza, L. A., Whiteman, E. L., Summers, S. A., and Birnbaum, M. J. (1999) *J. Biol. Chem. 274*, 24677−24684.
46. Favata, M. F., Horiuchi, K. Y., Manos, E. J., Daulerio, A. J., Stradley, D. A., Feeser, W. S., Van Dyk, D. E., Pitts, W. J., Earl, R. A., Hobbs, F., Copeland, R. A., Magolda, R. L., Scherle, P. A., and Trzaskos, J. M. (1998) *J. Biol. Chem. 273*, 18623−18632.
47. Hunter, T. (2000) *Cell 100*, 113−127.
48. Kruszynska, Y. T., and Olefsky, J. M. (1996) *J. Invest. Med. 44*, 413−428.
49. Haj, F. G., Verveer, P. J., Squire, A., Neel, B. G., and Bastiaens, P. I. (2002) *Science 295*, 1708−1711.
50. Kulas, D. T., Zhang, W.-R., Goldstein, B. J., Furlanetto, R. W., and Mooney, R. A. (1995) *J. Biol. Chem. 270*, 2435−2438.
51. Zhang, W.-R., Li, P.-M., Oswald, M. A., and Goldstein, B. J. (1996) *Mol. Endocrinol. 10*, 575−584.
52. Lammers, R., Moller, N. P., and Ullrich, A. (1997) *FEBS Lett. 404*, 37−40.
53. Zabolotny, J. M., Bence-Hanulec, K. K., Stricker-Krongrad, A., Haj, F., Wang, Y., Minokoshi, Y., Kim, Y. B., Elmquist, J. K., Tartaglia, L. A., Kahn, B. B., and Neel, B. G. (2002) *Dev. Cell 2*, 489−495.
54. Cheng, A., Uetani, N., Simoncic, P. D., Chaubey, V. P., Lee-Loy, A., McGlade, C. J., Kennedy, B. P., and Tremblay, M. L. (2002) *Dev. Cell 2*, 497−503.
55. Wiener, J. R., Kerns, B. J. M., Harvey, E. L., Conaway, M. R., Iglehart, J. D., Berchuck, A., and Bast, R. C., Jr. (1994) *J. Natl. Cancer Inst. 86*, 372−378.
56. Bjorge, J. D., Pang, A., and Fujita, D. J. (2000) *J. Biol. Chem. 275*, 41439−41446.
57. Liu, F., and Chernoff, J. (1997) *Biochem. J. 327*, 139−145.
58. Flint, A. J., Tiganis, T., Barford, D., and Tonks, N. K. (1997) *Proc. Natl. Acad. Sci. U.S.A. 94*, 1680−1685.
59. LaMontagne, K. R., Jr., Flint, A. J., Franza, B. R., Jr., Pandergast, A. M., and Tonks, N. K. (1998) *Mol. Cell. Biol. 18*, 2965−2975.
60. Balsamo, J., Arregui, C., Leung, T., and Lilien, J. (1998) *J. Cell Biol. 143*, 523−532.
61. Liu, F., Hill, D. E., and Chernoff, J. (1996) *J. Biol. Chem. 271*, 31290−31295.

BI035238P